Article

Multispectral Anti-Reflection Coatings Based on YbF$_3$/ZnS Materials on ZnGeP$_2$ Substrate by the IBS Method for Mid-IR Laser Applications

Mikhail Zinovev [1,2,*], Nikolay N. Yudin [1,2], Igor Kinyaevskiy [3], Sergey Podzyvalov [1,2], Vladimir Kuznetsov [2,4], Elena Slyunko [1,2], Houssain Baalbaki [1] and Denis Vlasov [1]

1 Laboratory for Radiophysical and Optical Methods of Environmental Studies, National Research Tomsk State University, 634050 Tomsk, Russia
2 Laboratory of Optical Crystals «LOC LLC», 634050 Tomsk, Russia
3 Lebedev Physical Institute of the Russian Academy of Sciences, 53 Leninskiy Pr., 119991 Moscow, Russia
4 Institute of High Current Electronics, Akademichesky av. 2/3, 634055 Tomsk, Russia
* Correspondence: muxa9229@gmail.com; Tel.: +7-952-158-37-58

Abstract: A multispectral anti-reflective coating of high radiation strength for laser applications in the IR spectrum for nonlinear ZnGeP$_2$ crystals has been developed for the first time. The coating was constructed using YbF$_3$/ZnS. The developed coating was obtained by a novel approach using ion-beam deposition of these materials on a ZnGeP$_2$ substrate. It has a high LIDT of more than 2 J/cm^2. Optimal layer deposition regimes were found for high film density and low absorption, and good adhesion of the coating to the substrate was achieved. At the same time, there was no dissociation of the double compound under high-energy ions.

Keywords: single crystal; ZnGeP$_2$; laser-induced damage threshold; crystal structure; optical coatings

1. Introduction

Ion-beam sputtering (IBS) is a well-studied and already proven method for obtaining thin oxide films, optical anti-reflection coatings (AR), and dielectric mirrors operating in visible and near-infrared spectral regions [1]. However, the absorption bands of oxide films in the range of 7–10 μm, due to the presence of ionic M–O bonds [2], limit the use of oxide materials for creating optical coatings operating in the mid-IR range. Many substrates used when working in the mid-IR spectrum have a high refractive index, and consequently, a strong reflection from the working surfaces. For example, an uncoated ZnGeP$_2$ crystal (hereinafter ZGP) has a refractive index of n = 3.14 and a reflection value of R ≈ 25% from the working face at a pump wavelength of 2.097 μm [3]. Therefore, to improve the energy characteristics of parametric frequency converters based on these crystals, anti-reflection optical coatings are used.

A group of chemical compounds based on sulfides (ZnS), selenides (ZnSe), and fluorides (ThF$_4$, MgF$_2$, YF$_3$, YbF$_3$), which have a transparency window of the order of 1–13 μm, are used to develop optical anti-reflection coatings in the mid-IR spectrum [4]. These materials have good adhesive properties, are non-hygroscopic, and have low absorption in the working wavelength band. Anti-reflection coatings for the mid-IR range based on the above materials are deposited by electron beam technology or by a magnetron source. These methods make it possible to achieve high rates of sputtering of the target material onto the substrate and ensure high productivity by coating a large number of substrates simultaneously. However, with this approach, thin films are not of the best quality; they have a low density due to the formation of pores during growth. The density of the film can be increased using an auxiliary-assisted ion source (the so-called IAD method), but this may increase the absorption of the film [5], so its use is not always justified. All the

above characteristics significantly affect the Laser-Induced Damage Threshold (LIDT) of thin films. Although the optical and adhesive properties of thin films have been studied, improving the LIDT of anti-reflection coatings is still a priority for the development of high-power mid-IR laser systems. High LIDT values can be achieved using the IBS method for applying near and mid-IR anti-reflection coatings [4,6].

Sputtering these materials by the IBS method has been shown in a few studies [7–9]. In our previous work [10], we had already shown the possibility of sputtering a ZnS ceramic target in the IBS setup. When using the IBS method, the films are dense with a higher refractive index compared to films obtained by a method such as IAD, and they have low absorption and good mechanical properties [4]. However, the high kinetic energy of particles during ion sputtering of the target can cause a destruction of the double compound into its components. Because of this, the stoichiometry of the film composition and optical parameters can be violated. Therefore, it is necessary to choose suitable parameters of the ion beam so that it is possible to spray sulfide and fluoride compounds without their destruction.

In this work, zinc sulfide (ZnS) was chosen for the high-refractive layer, and as a low-refractive layer, ytterbium fluoride YbF_3 [11]. The aim is to develop and apply an AR coating for the ZGP substrate, operating in the multispectral IR range of 2–3 µm and 7.5–8.5 µm wavelengths, which would have high LIDT values.

2. Sputtering Technique

The coatings were made on an Aspira-200 vacuum deposition machine (IZOVAC company, Belarus). The maximum substrate size is 200 mm in diameter with a maximum unevenness of up to ±2%. Up to four spray targets can be attached to the rotary water-cooled base at the same time. The maximum diameter of the targets is 101.6 mm, and the thickness of each is up to 10 mm. In our case we used ceramic target disks of ZnS and YbF3 (purity 99.99% or 4N for each) with 101.6 mm diameter and 6mm thickness, manufactured by Xing Kang Coating Materials, China. The gas supply system has electronic flow meters and valves. Gases are supplied to the system—especially pure argon (Ar 99.999%) and technically pure oxygen (O_2 99.7%). The ion source is an accelerator with an anode layer. Control of gas parameters and control of ion source parameters are carried out by the control computer of the vacuum unit. Compensation for the positive charge formed on the target surface during the deposition process is carried out using the thermal emission of electrons from a tungsten filament cathode.

In the vacuum unit, the gas supply is provided in two configurations: gas supplied directly into the vacuum chamber and gas supplied through the annular ion source. In the first case, the classical gas supply scheme is implemented, which is used in most vacuum deposition systems. In the case of the implementation of the second gas supply scheme, several advantages appear, including a lower residual pressure in the chamber compared to when the gas is admitted into the chamber volume. This entails an increase in the film deposition rate, since particles knocked out from the target reach the substrate region with a minimum probability of collision with gas molecules. In turn, this also results in denser films, which increases their optical stability by reducing the number of pores by which water and other contaminants can enter.

Before loading into the spray chamber, the substrates were cleaned using high-purity acetone and then washed with bi-distilled water. Immediately before coating in a vacuum chamber, the substrates were additionally cleaned with an auxiliary ion source at a source power of ~40 W and ion energy of ~150 eV for 10 min. Additionally, pure argon (Ar 99.999%) was used as a cleaning source. The substrate temperature was maintained at 100 °C throughout the entire deposition process.

3. Multilayer AR Coating Design

3.1. Single Layers Description

To begin with, the monolayers of materials were studied, from which later was developed an interference coating. The deposition parameters of the studied materials are presented in Table 1.

Table 1. Deposition parameters of the studied materials.

Sputtering Target	Accelerating Voltage of the Ion Source, kV	Layer Deposition Rate, nm/s	Residual Pressure in the Chamber at the Beginning of the Spraying Process, Pa	Working Pressure in the Chamber during Spraying, Pa	Used Gas/Flow, cm^3 per Minute
YbF_3	1.7	0.02	5×10^{-4}	5×10^{-2}	Ar/18
ZnS	2.5	0.045	5×10^{-4}	3.3×10^{-2}	Ar/15

Monolayers were described in a wide spectral range of 0.4–10 μm. The sputtering was carried out on various substrates: Asahi brand optical glass, BK8 glass and single crystal silicon wafers, and ZGP wafers. The thickness of the deposited monolayer was about 1 μm in order to obtain several interference peaks in the IR region and correct dispersion parameters. Then the transmission and reflection spectra of the studied monolayers were measured on two spectrometers. For the visible and near IR regions, a Shimadzu UV-3600Plus spectrometer (Kyoto, Japan) was used; for the mid-IR region, a Simex Fourier spectrometer (Novosibirsk, Russia) was used. Figure 1 shows that the obtained transmission and reflection spectra corresponds to the YbF_3 monolayer on the BK8 (Figure 1a) and ZGP (Figure 1b) substrates.
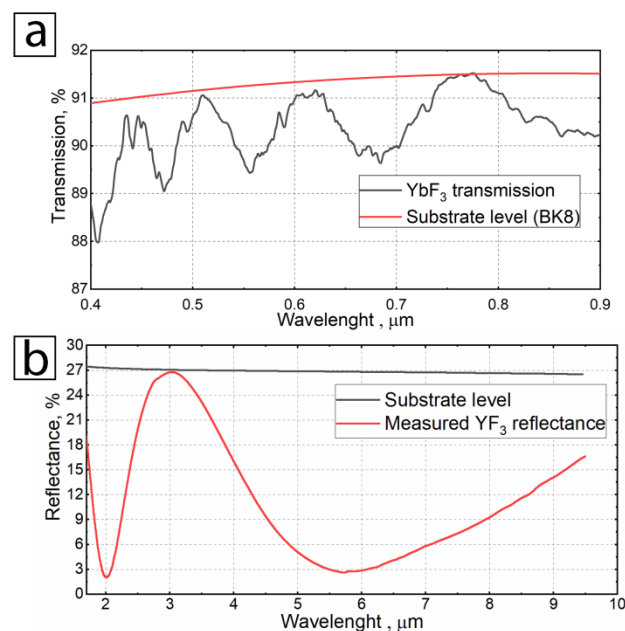

Figure 1. (**a**)—transmission spectrum of an YbF_3 monolayer on a BK8 substrate; (**b**)—reflection spectrum on a ZGP substrate.

Based on the obtained interference peaks, the refractive index dispersion of the YbF_3 monolayer, shown in Figure 2, was determined in the wide spectral range. The dispersion characteristics of both monolayers were calculated in the Optilayer software (version 15.12d) environment in the Optichar module.
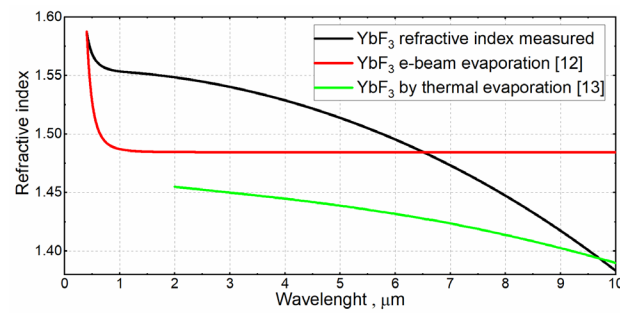
Figure 2. The black curve is the obtained refractive index dispersion of an YbF$_3$ monolayer by IBS method; the red curve is dispersion of an YbF3 film by e-beam evaporation taken from [12]; the green curve is dispersion of an YbF3 film by thermal evaporation taken from [13].

The dispersion characteristic agrees with the data obtained by the IBS method in [4]. At the same time, the refractive index of the obtained YbF$_3$ film is higher ($n \approx 1.55$ on 2 µm) than similar films which were obtained by the IAD method ($n \approx 1.48$ on 2 µm) in [12] and by the thermal evaporation method ($n \approx 1.46$ on 2 µm) in [13]. This fact indicates that the film obtained in this study by the IBS method is denser and less porous than those obtained by other methods of sputtering. From this point of view, such films may have greater resistance to LIDT, since they are less porous and therefore less hygroscopic and have better stoichiometry. In addition, the film is characterized by high transparency in the mid-IR range [12], but the absorption spectrum was not determined due to the used ZGP substrate having absorption in the mid-IR region.

Figure 3a,b shows the reflection spectrum of a ZnS monolayer on a BK8 substrate and a mono crystalline silicon substrate in the range of 0.4–10 µm.
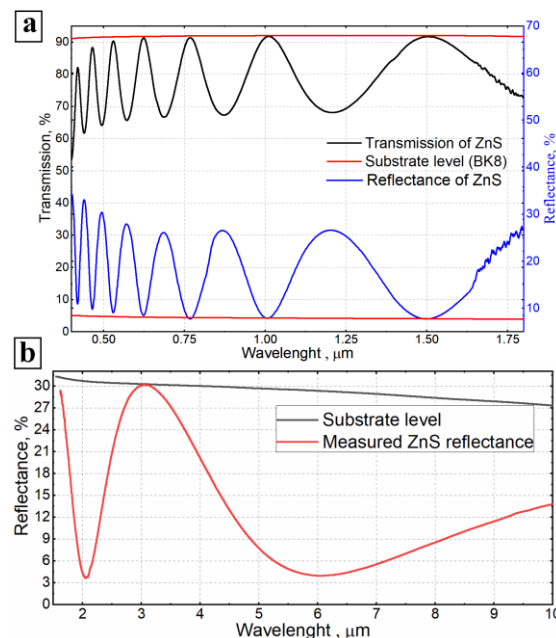

Figure 3. (**a**)—transmission and reflection spectra of a ZnS monolayer on BK8 substrate; (**b**)—reflection spectrum of a ZnS monolayer.

From the interference peaks, as for the YbF$_3$ monolayer, the optical dispersions of the refractive index and absorption coefficient of the ZnS monolayer were calculated, as shown in Figure 4.
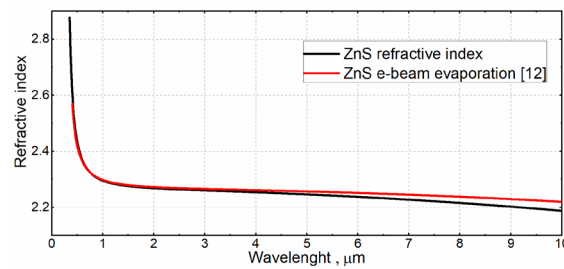
Figure 4. The black curve is the obtained refractive index dispersion of a ZnS monolayer by IBS method; the red curve is ZnS dispersion obtained in [12] by e-beam evaporation (IAD).

The characteristic of refractive index dispersion of a ZnS monolayer also agrees with the literature data [4,12–14]. The refractive index of the film deposited by the IBS method is slightly lower ($\Delta n \approx 0.2$) than that of the films obtained by the IAD and thermal evaporation methods. The absorption dispersion of the ZnS monolayer was determined only for visible and near IR spectrum. Strong absorption in the film begins only in the visible range at wavelengths shorter than 600 nm. In the mid-IR range from 1 to 10 μm, the film absorption was not determined due to the absence of correct measurements of transmission. Therefore, only dispersions of the refractive indices were determined for the films, which were subsequently used to calculate the target coating.

According to the analysis of the films' dispersion characteristics, the IBS method can be used to sputter these materials. With the optimal selection of the ion source parameters, the dissociation of the double compound molecules does not occur. The monolayers dispersion characteristics were used to calculate a multilayer anti-reflection coating on a ZGP substrate.

3.2. Designed Multilayer AR Coating

In this work, an anti-reflection coating on a ZGP substrate was designed, as a material used to create parametric light generators. OPO data can be used for various purposes, including remote gas analysis, medicine, etc. The anti-reflection coating presented in the article is multispectral. The coating consists of seven layers with a total thickness of 1305 nm. To improve the adhesion of the substrate coating and to reduce mechanical stresses, a low-refractive YbF_3 layer of small thickness ~40 nm was deposited as the first layer. The studied parameters of the coating and the obtained characteristics are shown in Table 2.

Table 2. Theoretical and experimental AR coatings parameters.

Pairs of Materials Used	Target Operating Range (Reflection no more than 1% Pump Area/No more than 2% OPO Area) in nm	Number of Layers in the Coating	Total Coating Thickness, nm
ZnS/YbF_3	2097; 2800–3000; 7500–8500.	7	1305

Figure 5 shows the curves of the calculated and measured reflection spectrum of the final coating.
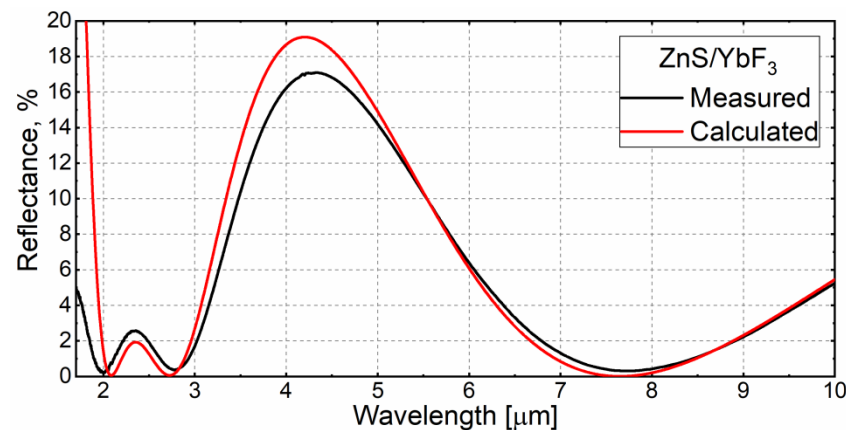
Figure 5. The calculated and measured reflection spectrum of the developed coating.

The red curve indicates the spectral reflection characteristics calculated in the Optilayer software environment. The target operating ranges of the coating for which the calculation was made are 2097 nm, 2800–3000, and 7500–8000 nm. The black curve in the figure indicates the measured spectrum of the obtained coating on the ZGP substrate. There are differences between the theoretical curve and the measured reflection spectrum, due to the absence of a quartz sensor for controlling the layer thickness in the spraying machine. The coating thickness is controlled only by the optical method and introduces an error when spraying the layer. This error can be summed up, and the finished coating has distinctions from the theoretical spectrum. It is also possible that there is an error in determining the refractive index of the materials used, and, consequently, the difference between the calculated characteristics of the coating and the real one. This error can occur, among other reasons, due to the fact that the measurement of the refractive index takes place in air, and the deposition in the chamber is in vacuum. Also, this error can be caused by the fact that the determination of the refractive index was made only by reflection in the IR region of the spectrum. There is also a slight difference in the absolute value of the reflection value of the measured film characteristic compared to the calculated one. We attribute this to the residual reflection from the second face of the sample, since it was matted with a finely dispersed grinding powder with a grain size of about 5 μm.

However, the sprayed coating fully complies with the target characteristics specified in the calculations. At the target wavelength of 2097 nm, the reflection is R ≤ 0.7%; in the range of 2800–3000 nm, the reflection is R ≤ 1.8%; and in the range of 6900–8900 nm, the reflectance does not exceed R ≤ 2%, with a reflection minimum of R ≤ 0.5% at λ = 7600 nm. The resulting coating fully matches the target requirements and can be used for anti-reflection of ZGP-based OPOs operating in the mid-IR range. However, another essential coating parameter is its LIDT, the results of which are presented below.

4. LIDT Test Method

LIDT testing of the obtained substrate/film system (SGP with applied anti-reflection coating based on alternating layers of ZnS/YbF$_3$) was conducted by a Ho^{3+}:YAG laser with parameters presented in Table 3.

Table 3. Ho^{3+}:YAG laser parameters.

Active Element Type	Wavelength, nm	Pulse Repetition Frequency, kHz	Pulse Duration, ns	Average Power, W
Solid State Ho^{3+}:YAG	2097	10–20	35 ns	1–20

The scheme of the experimental setup is shown in Figure 6. The measured diameter of the focused spot of the Ho^{3+}:YAG laser radiation at the input aperture of the test sample

in all experiments was d = 350 $\pm$ 10 μm at the e^{-2} level from the maximum intensity. The power of the incident laser radiation was changed using an attenuator consisting of a half-wave plate ($\lambda/2$) and a Glan polarization prism (BSC). A Faraday insulator (F.I.) was used to prevent reflected radiation from entering the laser, which prevented uncontrolled changes in the parameters of the affected radiation. The average power of the laser radiation (P_{av}) was measured before each experiment with an Ophir power meter (P.M.).
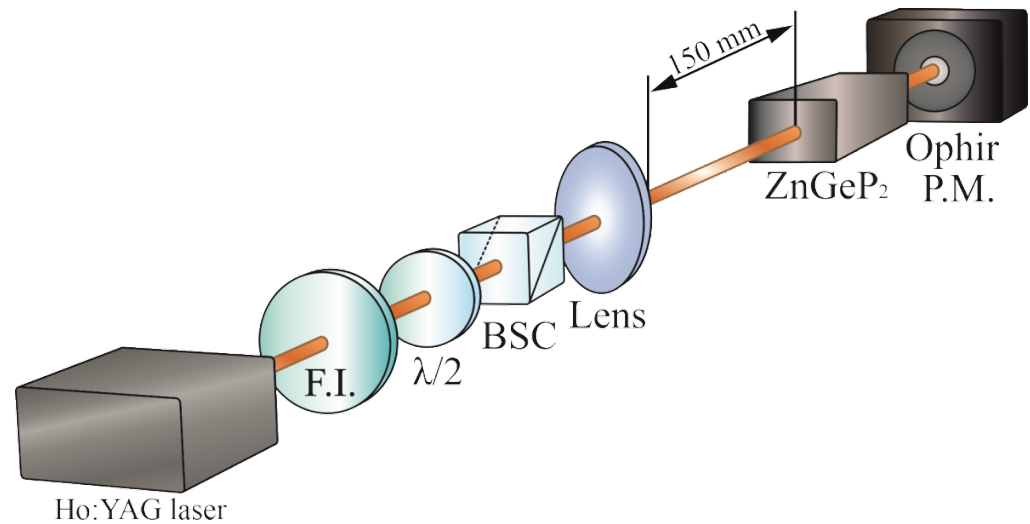

Figure 6. Scheme of the experimental setup for determining LIDT.

According to the international standard ISO 11146 [15], the energy density of laser radiation and the power density were determined by the following expressions:

$$W = 8P_{av}/(f\pi d^2), \tag{1}$$

$$P = 8P_{av}/(\tau f\pi d^2), \tag{2}$$

where d is the diameter of the laser beam, f is the pulse repetition frequency, and τ is the duration of the laser pulses.

To determine the optical breakdown threshold of the samples, the "R-on-1" method was used, which requires less space on the sample surface compared to the "S-on-1" method and, therefore, can be applied to samples with a limited aperture, although it is considered rougher [16]. The essence of this technique is that each region of the crystal is irradiated with laser radiation with a sequential increase in the intensity of laser radiation, until an optical breakdown occurs or a predetermined energy density value is reached. In our work, the study was carried out with exposure duration τ_{ex} = 5 s. The sample under study was exposed to packets of laser pulses with a fixed level of energy density, which did not cause damage to the surface of the crystals. Further, the level of energy density increased with a step of ~0.1 J/cm^2. When visible damage appeared on one of the surfaces of the nonlinear element, the experiment was terminated. Then the sample was moved by 0.5 mm in height or width using a two-coordinate shift; the experiment was repeated five times. The optical breakdown probability was obtained by plotting the cumulative probability as a function of the optical breakdown energy density. The value of the optical breakdown threshold (W_{0d}) was taken to be the energy density corresponding to the approximation of the probability of optical breakdown to zero. Figure 7 shows the results of measuring the optical breakdown threshold using the R-on-1 method. In the presented graphs, the probability of optical breakdown in relative units, normalized to unity, is plotted along the ordinate axis, and the energy density of the testing laser radiation is plotted along the abscissa axis.
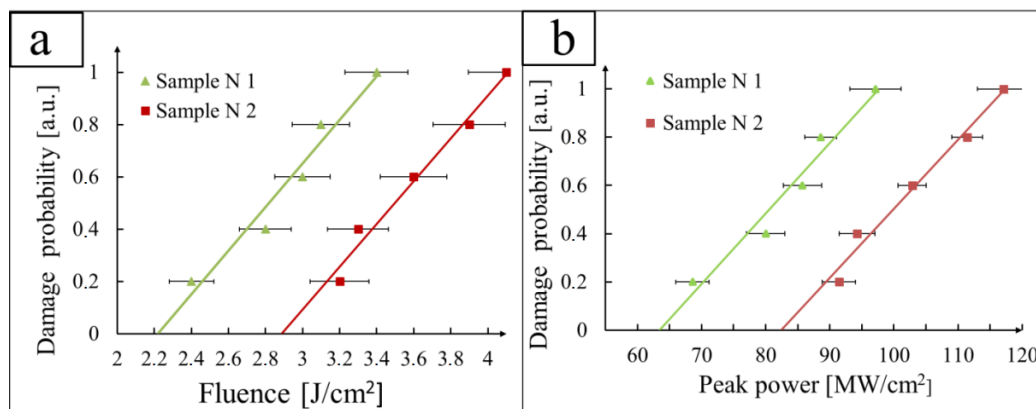
Figure 7. Dependence of the optical breakdown probability of samples No. 1 and No. 2 on the energy density of the incident laser radiation—(**a**); and on the power density of the incident laser radiation—(**b**).

5. Experimental Results of LIDT Test and Discussion

According to the R-on-1 method, using the experimental stand shown in Figure 6, the values of the optical breakdown threshold of ZGP samples No. 1 (without anti-reflection coatings) and No. 2 (with a coating based on alternating YbF_3 and ZnS layers) were determined (Figure 7). The standard deviation of the LIDT determination was ± 0.1 J/cm^2.

According to the experimental data, the LIDT of the ZGP sample No. 1 (without anti-reflection coatings) was W_{0d} = 2.2 $\pm$ 0.1 J/cm^2 (64 MW/cm^2). The LIDT of sample No. 2 (with YbF_3/ZnS anti-reflection coating) was W_{0d} =2.9 $\pm$ 0.1 J/cm^2 (83 MW/cm^2). The growth of LIDT upon deposition of an anti-reflection coating on single crystal ZGP was 32%. The studied samples had a low absorption at the exposure wavelength (0.03 cm^{-1} at a wavelength of 2097 nm), which indicates a low concentration of point defects affecting the absorption intensity [17,18]. The presence of binary phosphides [18], impurity elements [18], and bulk defects (by the digital holography method [19]) was not found in all the samples studied, which indicated a qualitative stoichiometric crystal structure of a single crystal. Since both samples were cut from the same ingot, the obtained data of the difference in the optical breakdown threshold of samples No. 1 and No. 2 can be explained by the applied coating. A similar trend towards an increase in LIDT during the deposition of optical coatings was observed in the work [20]. The authors of the work found that the deposition of an antireflection coating on the ZGP crystal leads to an increase in LIDT by a factor of 2 from 1 J/cm^2 to 2 J/cm^2. However, in this work, there are no data on the applied interference coating, so we are unable to compare it directly.

The anti-reflection coating, characterized by good adhesion to the polished surface of the crystal and compensated internal stresses, leads to an increase in the threshold of optical breakdown compared to an unenlightened sample. In turn, this occurs due to the "closing" of broken chemical bonds and bulk defects emerging on the polished surface of the crystal.

6. Conclusions

The achieved studies have shown the possibility of sputtering ZnS and YbF_3 ceramic targets by the IBS method onto the ZGP substrate. The monolayers had a high refractive index compared to the films obtained by the e-beam and IAD methods. Extremely low film absorption is also shown over the entire operating range. The optimal parameters of the ion source were selected, wherein the dissociation of the double compound into its components does not occur. Based on the dispersion characteristics of the monolayers, a multispectral anti-reflection coating was developed for the mid-IR range. ZGP material was used as a substrate. It is shown that the anti-reflection coating increases the LIDT of a single crystal by up to 32%, from 2.2 $\pm$ 0.1 J/cm^2 to 2.9 $\pm$ 0.1 J/cm^2.

The developed coating is multispectral, has low absorption and high LIDT, and can also be used for deposition on various crystalline and amorphous substrates in the IR range.

References

1. Kolodnyi, G.Y.; Azarova, V.V.; Golyaev, Y.D.; Melnikov, A.; Rasyov, M.; Tikhmenev, N. Low-loss IBS mirrors for Zeeman laser gyros. *Proc. SPIE* **1999**, *3738*, 446–452. [CrossRef]
2. Wachs, I.E. Raman and IR studies of surface metal oxide species on oxide supports: Supported metal oxide catalysts. *Catal. Today* **1996**, *27*, 437–455. [CrossRef]
3. Zelmon, D.E.; Hanning, E.A.; Schunemann, P.G. Refractive-index measurements and Sellmeier coefficients for zinc germanium phosphide from 2 to 9 μm with implications for phase matching in optical frequency-conversion devices. *J. Opt. Soc. Am.* **2001**, *18*, 1307–1310. [CrossRef]
4. Ribeaud, A.; Pistner, J.; Hagedorn, H.; Joseph, S. Infra-Red Multi-Layer Coatings Using YbF3 and ZnS in an Ion Beam Sputtering System. In Proceedings of the Optical Interference Coatings Conference (OIC) 2019, Santa Ana Pueblo, NM, USA, 2–7 June 2019; Statespaper MC.7. pp. 1–4. [CrossRef]
5. Zhang, Y.; Xiong, S.; Huang, W.; Zhang, K. Determination of refractive index and thickness of YbF_3 thin films deposited at different bias voltages of APS ion source from spectrophotometric methods. *Adv. Opt. Technol.* **2018**, *7*, 33–37. [CrossRef]
6. Yudin, N.N.; Zinoviev, M.; Gladkiy, V.; Moskvichev, E.; Kinyaevsky, I.; Podzyvalov, S.; Slyunko, E.; Zhuravleva, E.; Pfaf, A.; Yudin, N.A.; et al. Influence of the Characteristics of Multilayer Interference Antireflection Coatings Based on Nb, Si, and Al Oxides on the Laser-Induced Damage Threshold of $ZnGeP_2$ Single Crystal. *Crystals* **2021**, *11*, 1549. [CrossRef]
7. Kennedy, J.; Murmu, P.P.; Gupta, P.S.; Carder, D.A.; Chong, S.V.; Leveneur, J.; Rubanov, S. Effects of annealing on the structural and optical properties of zinc sulfide thin films deposited by ion beam sputtering. *Mater. Sci. Semicond. Process.* **2014**, *26*, 561–566. [CrossRef]
8. Yudin, N.N.; Antipov, O.L.; Gribenyukov, A.I.; Dyomin, V.V.; Zinoviev, M.M.; Podzyvalov, S.N.; Slyunko, E.S.; Zhuravleva, E.V.; Pfeif, A.A.; Yudin, N.A.; et al. Influence of Postgrowth Processing Technology on the Laser Induced Damage Threshold of $ZnGeP_2$ Single Crystal. *Russ. Phys. J.* **2022**, *64*, 2096–2101. [CrossRef]
9. Zhang, J.; Sun, D.G.; Fu, X.H.; Liu, D.M. Study and Fabrication of Multi-Band Filter Film on ZnS Substrate. *Key Eng. Mater.* **2013**, *552*, 147–151. [CrossRef]
10. Zinoviev, M.; Yudin, N.N.; Podzvalov, S.; Slyunko, E.; Yudin, N.A.; Kulesh, M.; Dorofeev, I.; Baalbaki, H. Optical AR Coatings of the Mid-IR Band for $ZnGeP_2$ Single Crystals Based on ZnS and Oxide Aluminum. *Crystals* **2022**, *12*, 1169. [CrossRef]
11. Zhang, Y.; Fan, J.; Long, G. Influence of deposition parameters on residual stress of YbF_3 thin film. *Proc. SPIE* **2015**, *9796*, 97960N. [CrossRef]
12. Amotchkina, T.; Trubetskov, M.; Hahner, D.; Pervak, V. Characterization of e-beam evaporated Ge, YbF_3, ZnS, and LaF_3 thin films for laser-oriented coatings. *Appl. Opt.* **2020**, *59*, A40–A47. [CrossRef] [PubMed]
13. Zhang, Y.; Zhang, K.; Huang, W.; Xiong, S. Determination of infrared refractive index of ZnS and YbF_3 thin films by spectroscopy. *Optik* **2018**, *170*, 321–327. [CrossRef]
14. Nadeem, M.Y.; Ahmed, W. Optical Properties of ZnS Thin Films. *Turk. J. Phys.* **2000**, *24*, 651–659. Available online: https://journals.tubitak.gov.tr/physics/vol24/iss5/6 (accessed on 3 October 2022).
15. *ISO11146-1:2005*; Lasers and Laser-Related Equipment—Test Methods for Laser Beam Widths, Divergence Angles and Beam Propagation Ratios—Part 1: Stigmatic and Simple Astigmatic Beams. ISO: Geneva, Switzerland, 2005. Available online: https://www.iso.org/standard/33625.html (accessed on 3 October 2022).

16. The R-on-1 Test. *Lidaris LIDT Service*. 2019. Available online: https://lidaris.com/laser-damage-testing/r-on-1-test (accessed on 3 October 2022).
17. Gribenyukov, A.I.; Podzyvalov, S.N.; Soldatov, A.N.; Shumeiko, A.S.; Yudin, N.A.; Yudin, N.N.; Yurin, V.Y. Defectoscopy of ZnGeP$_2$ single crystals using a strontium vapour laser. *Quantum Electron.* **2018**, *48*, 491–494. [CrossRef]
18. Yudin, N.N.; Antipov, O.L.; Gribenyukov, A.I.; Eranov, I.D.; Podzyvalov, S.N.; Zinoviev, M.M.; Voronin, L.A.; Zhuravleva, E.V.; Zykova, M.P. Effect of postgrowth processing technology and laser radiation parameters at wavelengths of 2091 and 1064 nm on the laser-induced damage threshold in ZnGeP$_2$ single crystal. *Quantum Electron.* **2021**, *51*, 306–316. [CrossRef]
19. Dyomin, V.V.; Gribenyukov, A.I.; Davydova, A.Y.; Olshukov, A.S.; Polovtsev, I.G.; Podzyvalov, S.N.; Yudin, N.N.; Zinovev, M.M. Visualization of volumetric defects and dynamic processes in crystals by digital IR-holography. *Appl. Opt.* **2021**, *60*, A296–A305. [CrossRef] [PubMed]
20. Zawilski, K.T.; Setzler, S.D.; Schunemann, P.G.; Pollak, T.M. Increasing the laser-induced damage threshold of single-crystal ZnGeP$_2$. *J. Opt. Soc. Am. B* **2006**, *23*, 2310–2316. [CrossRef]